Preprint Title	Nickel nanoparticle decorated reduced graphene oxide-WO3 nanocomposite - a promising candidate for gas sensing
Authors	Ilka Simon, Alexandr Savitsky, Rolf Mülhaupt, Vladimir Pankov and Christoph Janiak
Publication Date	21 Dez. 2020
Article Type	Full Research Paper
Supporting Information File 1	Ni@rGO+WO3_SI_BJNano.docx; 29.9 KB
ORCID® iDs	Vladimir Pankov - https://orcid.org/0000-0001-5478-0194; Christoph Janiak - https://orcid.org/0000-0002-6288-9605

Nickel nanoparticle decorated reduced graphene oxide-WO_3 nanocomposite - a promising candidate for gas sensing

Ilka Simon,[1] Alexandr Savitsky,[2] Rolf Mülhaupt,[3] Vladimir Pankov,*[2] and Christoph Janiak*[1]

Adresse:

[1] Institut für Anorganische Chemie und Strukturchemie, Heinrich-Heine-Universität Düsseldorf, 40204 Düsseldorf, Germany. Fax: +49-211-81-12287; Tel: +49-211-81-12286.

Email: Christoph Janiak – janiak@uni-duesseldorf.de

[2] Chemical Faculty, Belarusian State University, Lenningradskaya str. 14, 220050 Minsk, Belarus

Email: Vladimir Pankov – pankov@bsu.by

[3] Freiburg Materials Research Center and Institute for Macromolecular Chemistry, Albert-Ludwigs-University Freiburg, 79104 Freiburg, Germany

* Corresponding author

Abstract

We report for the first time the doping of WO_3 sensing elements with a non-noble metal carbon composite, namely a nickel metal nanoparticle-carbon composite (Ni@rGO). Previous work with WO_3 had used either NiO (as part of the WO_3 lattice) or carbon alone or Pd-surface decorated WO_3 (Pd@WO_3) or Pd or Pt@carbon@WO_3. We demonstrate the gas response for pure WO_3, rGO-doped WO_3 and Ni@rGO doped WO_3 sensing elements towards NO_2 (10 ppm) and acetone (35,000 ppm) in air. The addition of 0.35 wt% Ni@rGO composite to WO_3 enables the increase of the sensory response by more than 1.6 times for NO_2 vapors as well as 4 times regarding acetone vapors (*n*-type response).

Keywords

gas sensing, magnetic measurements, nickel nanoparticles, reduced graphene oxide, tungsten oxide

Introduction

Toxic gases as well as volatile organic compounds (VOC) are known air pollutants and their emissions are harmful for humans and the ecosystem [1]. Sensor materials which can detect the type and concentration of these gases are therefore needed in various kinds of environments and industries [2]. A gas sensor should be highly sensitivities and highly selective with a fast response and recovery rate and should work at low cost and low power consumption [3]. In comparison to conventional gas sensors, nanostructure based gas sensors are more sensitive, because of their increased detection area [4]. Most commonly for gas sensing the resistance mode is used, where the change in sensor resistance with exposure to the interacting gas is measured directly [5]. Gases can either be oxidizing like NO, N_2O NO_2, O_3, Cl_2 or reducing like H_2S, NH_3, CO, H_2, SO_2, CH_4, or rather inert like CO_2 [6,7]. VOCs are organic molecules like acetone, ethanol and formaldehyde [8,9].

Metal oxide semiconductors (MOS) are the most widely used gas sensors [10]. MOS can be divided into *n*-type and *p*-type MOS. In *n*-type MOS electrons are the major charge carriers wherein in *p*-type MOS holes are the major charge carriers [6]. The exposure to reducing gases cause a decrease in resistance in *n*-type MOS and an increase in *p*-type MOS. On the other hand, the exposure to oxidizing gases lead to an increase in resistance for *n*-type MOS and a decrease for *p*-type MOS [8]. MOS have certain advantages like a fast response time and an excellent sensitivity towards all kinds of gases [11]. The major disadvantages of MOS are their poor selectivity and high operating temperatures of 200 to 400 °C, which means a higher power consumption [4]. WO_3 is a wide band-gap [12,13] *n*-type semiconductor [14,15] with good sensitivity towards NO_2 [16] as well as CO [17].

Known successful routes to improve the MOS gas sensing performance are doping with transition metals, decoration with noble metals, formation of heterojunctions or size reduction [18,19]. Doping with nickel in WO_3 improves the humidity sensing properties compared to neat

WO_3. Attributed to a greater number of electrons donated by Ni atoms, higher surface area and small band gap energy, Ni-doped WO_3 has a faster response, higher sensitivity, and greater stability than pure WO_3 [20]. The decoration of palladium nanoparticles on the surface of WO_3 can be used as an improved and reusable gas sensor for NH_3 [21].

Metal oxide-semiconductor junctions can either be formed between two *p*-type MOS as well as two *n*-type MOS (*p*-*p*/*n*-*n*-homojunctions) or between a *p*-type MOS and an *n*-type MOS (*p*-*n*-heterojunctions) [6,18]. *p*-Type MOS NiO on its own is not a very popular gas sensing material, because *p*-type MOS have in general a lower gas response than *n*-type MOS like WO_3, ZnO or SnO_2 [22,23]. But *p*-type MOS are ideal doping agents [24]. If *p*-type NiO is combined with *n*-type WO_3 they form a *p*-*n*-heterojunction, which improved their gas sensing abilities significantly [25].

Carbon based materials are also promising gas sensors, because of their high surface area, high chemical and thermal stability [26,27]. Pristine graphene is a good conductor, but rather inactive for gas sorption, because it has only a few functional groups on its surface which limits the chemisorption of gas molecules [28]. Graphene oxide (graphite oxide, GO) on the other hand has numerous oxygen functionalities and few remaining π-bonds and is therefore electrically insulating [29]. GO can be reduced (rGO) chemically or thermally. Through the partial removal of oxygen groups, the conductivity can be restored. Additionally, defects and vacancies are created [26]. Because of the ultra-high surface area per atom and the high electron transport along the graphene plane, rGO has a rapid and high response to gas molecules at room temperature [30]. Disadvantages of rGO gas sensors are the long recovery time, because of the high binding force between gas molecules and the graphene material [31]. rGO is a *p*-type semiconductor and can be used for gas sensing of low concentrations of NO_2 at room temperature [32].

The combination of MOS with graphene materials can have synergistic effects to improve their individual gas sensing abilities [33,34]. MOS prevent graphene from agglomerating, which lead to a higher specific surface area. Graphene on the other hand can control the size and morphology of MOS during the synthesis and decreases the resistance of MOS which leads to a rapid electron transfer from the surface reaction of the target gas with the MOS to the electrodes [35]. Additionally, MOS and graphene can form junctions at their interface. *P*-*p*-Homojunctions can, e.g., be formed between NiO and rGO to increase the gas sensing responsivity and sensitivity towards NO_2 gas [36]. In the combination of WO_3 and rGO *p*-*n*-heterojunctions are formed. This leads to an increased NO_2 response at room temperature [37]. Overall MOS@rGO gas sensors are more selective and sensitive with a faster response and recovery rate even at room temperature [8].

The sensing performance of MOS@rGO can further be improved by either chemical doping as well as compositing with a transition metal as ternary component [38]. Iron oxide doped WO_3 films showed improved NO_2 sensing at room temperature, when adding a layer of 16 nm *p*-type rGO on the metal oxide film [39]. Nickel doped SnO_2 nanoparticles loaded with graphene have an enhanced acetone response at 350 °C with increased graphene loading level (best at 5 wt% graphene) [40]. Nickel and rGO doped ZnO nanostructures were used for hydrogen sensing at 100 °C [34].

The decoration of a MOS with a noble metal like Pd or Pt improves the sensitivity, response time and working temperature of MOS/rGO systems [15,41]. Pd and Pt nanoparticle decorated TiO_2/rGO were successfully used in the gas sensing of hydrogen gas [42]. The decoration of WO_3/rGO-nanosheets with Pt-nanoparticles achieved a faster response for acetone at 200 °C [43]. With the addition of Ag-nanoparticles to a dispersion of SnO_2/rGO the working temperature was dropped from 55 °C to room temperature in the gas sensing of NO_2 [44]. (For further examples and comparison with other gas sensors see table 1 in the ESI).

The ternary Ni@rGO-WO_3 nanocomposite was synthesized and tested in comparison to pure WO_3 and rGO@WO_3 towards the gas response of the oxidizing gas NO_2 (10 ppm in air) and the VOC acetone (35,000 ppm in air).

Results and Discussion

Nanoparticle synthesis

The synthesis of nickel nanoparticles is well known through the literature using different methods such as thermal decomposition [45] or reductive hydrogenation [46]. Nickel nanoparticles can easily be synthesized from the precursor material $Ni(COD)_2$ in different ionic liquids with sizes below 10 nm without any additional stabilizing or reducing agents [47]. Ionic liquids have the ability to exfoliate the graphene oxide into single sheets hence a higher surface area can be achieved [48]. Thermally reduced graphene oxide (rGO) was tested before with different metals in ionic liquids [49,50]. The preparation of nanoparticles decorated on rGO can be achieved in situ or by mixing the previously prepared solutions [51].

Here, we choose the ionic liquid [BMIm][NTf_2], an in situ microwave decomposition approach with rGO synthesized from reduced graphite oxide at 400 °C. It is extremely important that the used rGO is thoroughly dried because of the oxyphilic nature of nickel nanoparticles. Therefore, before the nanoparticle synthesis, the rGO was dried using a turbo molecular pump at $5*10^{-7}$ mbar for several days. Then rGO was dispersed with $Ni(COD)_2$ in [BMIm][NTf_2] to gain 0.5 wt-% metal nanoparticles and 0.5 wt-% rGO. In order to stir the reaction during the microwave decomposition, 0.5 wt% rGO could not be exceeded. The obtained nanomaterial was analyzed using powder diffraction (P-XRD). The powder pattern shows the reflexes for hexagonal nickel (Figure 1).

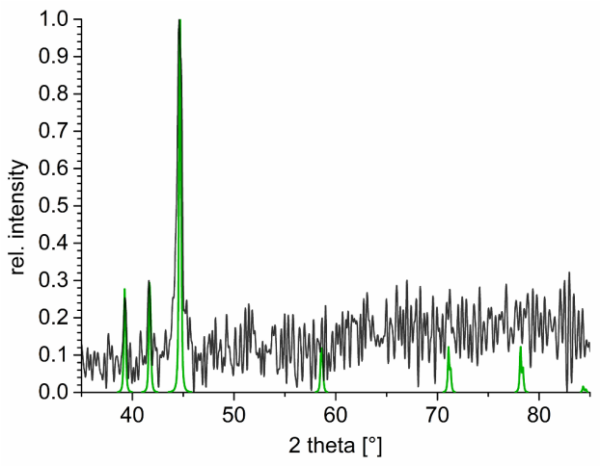

Figure 1: Powder-pattern and particle size distribution of nickel nanoparticles@rGO from 0.5 wt% dispersion of from $Ni(COD)_2$ in $[BMIm][NTf_2]$ (Ni space group: *P* 6_3/*mmc*).

TEM-images show spherical nickel nanoparticles which are supported on top of rGO (Figure 2). The particles have a size distribution of 25 ± 5 nm. All nanoparticles were supported on the rGO. The particle size of Ni@rGO increased in comparison to pure nickel nanoparticles from $[BMIm][NTf_2]$ (size pure nickel nanoparticles 11± 2 nm) [47]. Nickel nanoparticles supported on pristine graphene sheets were synthesized with 35 ± 5 nm [52].

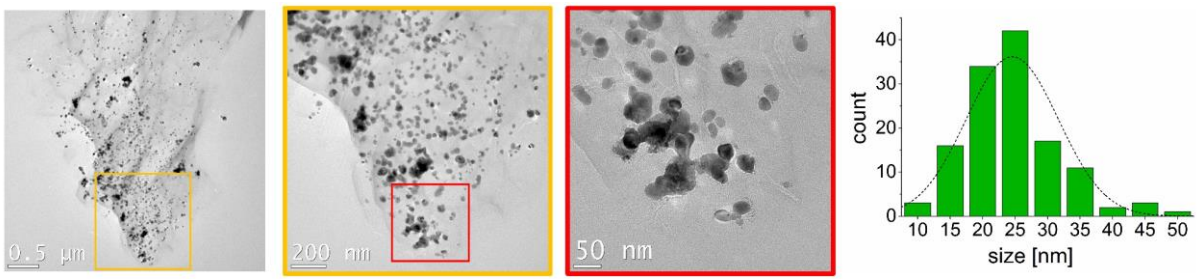

Figure 2: TEM-images of nickel nanoparticles@rGO from 0.5 wt% dispersion of from $Ni(COD)_2$ in $[BMIm][NTf_2]$. Particle size distribution of 25 ± 5 nm.

The nickel content was measured using atomic absorption spectroscopy (AAS). Nickel nanoparticles@rGO contained 8 % nickel. The metal loading on graphene oxide between 5 % – 20 % is common [50].

Gas sensing measurements on gas permeable pellets

The Ni@rGO doping of WO_3 samples were a mixture of the WO_3 xerogel and Ni@rGO pressed as pellets. Dry air was used as a reference gas. The electrical resistance was measured for the testing gas mixture and air. The response of a semiconductor sensor is the ratio of electrical resistance in air and in a gas medium. In the presence of reducing gases (e.g. acetone vapor), the sensor resistance decreases. In the presence of oxidizing gases (e.g., NO_2), the electrical resistance increases [7].

At 239 ˚C the electrical resistance of the 0.35 wt% Ni@rGO/WO_3 sample to 35,000 ppm acetone in air for 10 minutes decreased more than 4 times (from 74.0 to 17.8 kΩ, Figure 3) , while the electrical resistance of the WO_3 sample without additive changed less, from 7.1 to 1.9 kΩ.

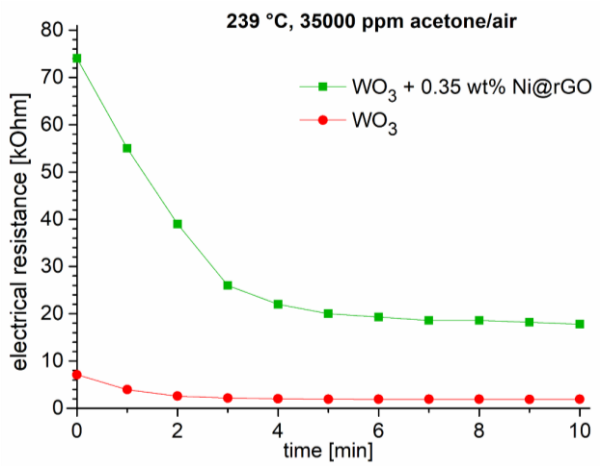

Figure 3: Time dependence of the sensor resistance values of the WO_3 and 0.35 wt% Ni@rGO/WO_3 samples under exposure to an acetone vapor in air mixture at 35,000 ppm.

At 240 ˚C the electrical resistance of the 0.35 wt% Ni@rGO/WO_3 sample in a gas-air environment containing 10 ppm NO_2 increased 1.6 times (from 17.6 to 27.6 kΩ, Figure 4).

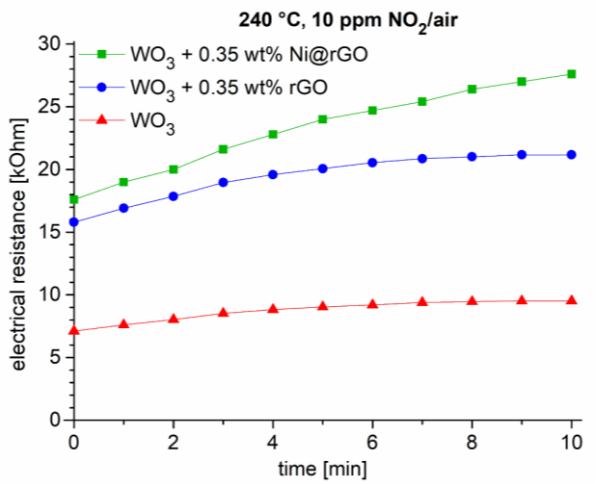

Figure 4: Time dependence of the sensor resistance values of the WO_3, rGO/WO_3 and 0.35 wt% Ni@rGO/WO_3 samples under exposure to a gas mixture containing 10 ppm NO_2 in air.

Thus, the addition of Ni@rGO to WO_3 enables the increase of the sensory response to NO_2 and acetone vapors (*n*-type response).

In contrast to sensors, where the sensing element consists only of rGO, sensors based on semiconductor oxide compositions, for example WO_3 with rGO have a higher response and shorter response-recovery times. In the case of pure rGO, the restoration of the original parameters of the sensors may not be observed at all.[8] In addition, oxide-based composites are mechanically more durable, and manufacturing mass sensors based on them seems to be more economically feasible due to the low content of graphene in the sensing element (up to several percent).

At present, there is no generally accepted mechanism of gas sensitivity of semiconductor oxide compositions with graphene. The reasons for the increase in the response and decrease in the operating temperature of the oxide composition containing unoxidized graphene are

indicated by the synergetic effect between graphene and metal oxides as a result of the occurrence of chemical bonds between graphene and metal oxides. In the case of reduced graphene oxide (semiconductor), various reasons are considered, such as the appearance of *p-n* junctions that shift the Fermi level of the oxide. There is evidence of effective charge transfer between graphene and nanospheres through chemical bonds. Emergence of conducting channels from graphene layers is also pointed out, which increase the efficiency of charge carrier transfer in composites.[8]

Magnetic measurements

In order to investigate if a nickel oxidation had occurred in the Ni@rGO composite along with its heat treatment in the study of sensory properties (250 °C), the following model experiment was performed. The original Ni@rGO composite was annealed at a temperature of 250 °C for two hours. In the following, its magnetic properties, namely the Curie temperature from the temperature dependences of magnetization and magnetic susceptibility were determined.

The results of the magnetic analysis (Figure 5a) indicate that the magnetic phase in the Ni@rGO composite is pure nickel. The Curie temperatures of the composite (T_c = 630 K) and the reference value for pure nickel [53] coincide (Figure 5 a,b). Moreover, the amount of magnetic phase in the Ni@rGO composite, as shown by magnetization measurements, corresponds to 7.8 wt%. The same amount of nickel is present in the original Ni@rGO composite without heat treatment.

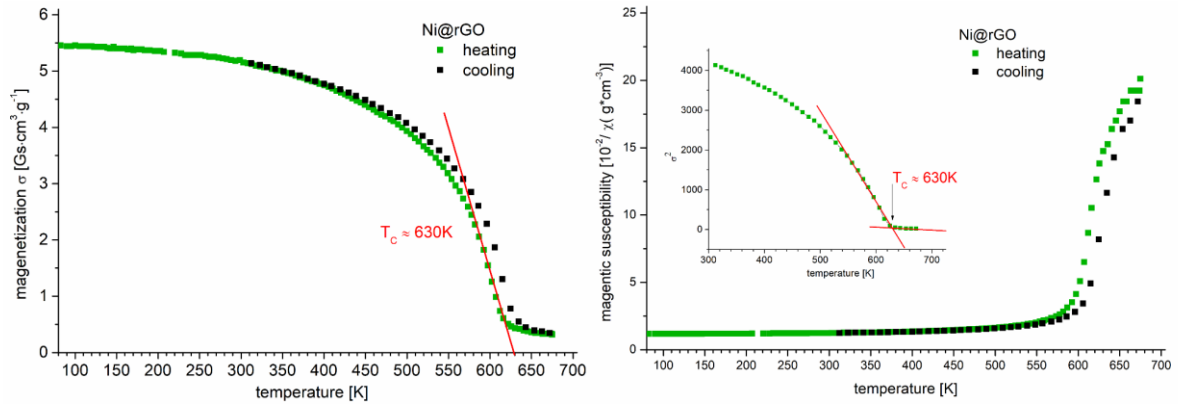

Figure 5: a) Magnetization versus temperature for the Ni@rGO composite in argon atmosphere b) Magnetic susceptibility versus temperature for nickel in argon atmosphere.

Thus, the results of measurements of the magnetic susceptibility and magnetization indicate the presence of only a metallic nickel phase in the Ni@rGO composite after its heat treatment in air.

Conclusion

Ni@rGO nanocomposites were found to be promising materials that enable the preparation of WO_3 gas and vapor sensor elements with improved sensory response. The addition of a very small amount of Ni@rGO (0.35 wt%) to WO_3 increases the gas response regarding NO_2 traces and acetone vapors in air significantly compared to the WO_3 element without the metal-graphene oxide dopant. The facile preparation of nickel nanoparticles supported on reduced graphene oxide opens the door for its application also as a dopant towards other metal oxide gas sensors.

Experimental

Due to the sensitivity of the precursor substances towards moisture and oxidation, all experiments were carried out in a purified argon (grade 99.998 vol.-%) or nitrogen (grade 99.996 vol.-%) atmosphere by using standard Schlenk techniques. Samples were prepared and stored in a MBraun Glovebox. Used solvents (acetonitrile, *n*-hexane, methylene chloride) were dried by using a MBraun solvent purification system or distilled (1-methylimidazole, 1-chlorobutane) and stored over 4 Å molecular sieves in a nitrogen atmosphere. Final water contents measured by coulometric Karl Fischer titration (ECH/ANALYTIK JENA AQUA 40.00) did not exceed 10 ppm.

$Ni(COD)_2$ was purchased from ABCR , stored at −4 °C and used without further purification. The ionic liquid [BMIm][NTf_2] was synthesized according to literature by reacting 1-methylimidazole with 1-chlorobutane to yield first [BMIm][Cl] which was further reacted with $LiNTf_2$ to give [BMIm][NTf_2] [54,55]. The IL was dried in a turbo molecular pump vacuum (10^{-7} mbar) at 80 °C for three days. Characterization was carried out by ^{1}H- and ^{13}C-NMR. Quantitative anion exchange and IL purity of 99,9 % was assessed by ion chromatography (Dionex ICS-1100, with IonPac® AS22, 4 x 250 mm column). Water content measured by coulometric Karl Fischer titration was below 10 ppm. rGO was synthesized in a two-step oxidation and thermal reduction process using natural graphite (type KFL 99.5 from AMG Mining AG, former Kropfmühl AG, Passau, Germany) as starting material. The graphite was oxidized according to literature [56]. Reduction of the graphite oxide were performed at 400 °C. Before using rGO in the nanoparticle synthesis, it was dried at 100 °C using a turbo molecular pump at $5 \cdot 10^{-7}$ mbar for several days.

Powder X-ray diffraction, PXRD data were measured at ambient temperature on a Bruker D2 Phaser using a flat sample holder and Cu–Kα radiation (*λ* = 1.54182 Å, 35 kV). Samples had been precipitated with acetonitrile from the nanoparticle/ionic liquid dispersion and washed several times with acetonitrile. PXRDs were measured for 1 h (5 to 100° 2theta).

Atomic absorption spectroscopy, AAS for metal analysis were performed on a PerkinElmer PinAAcle 900T, equipped with a flame furnace. Flame-AAS with an air-acetylene flame was used for the determination of the nickel content. Samples were digested in hot aqua regia two times (30 mL). The residues were re-dissolved in aqua regia, filtered and brought with water to a total volume of 10 mL. For the nickel measurements the samples were diluted 1 : 100.

Transmission electron microscopy, TEM was performed with a FEI Tecnai G2 F20 electron microscope [57] operated at 200 kV accelerating voltage or FEI Titan 80-300 TEM operated at 300 kV accelerating voltage [58]. Conventional TEM images were recorded with a Gatan UltraScan 1000P detector. TEM samples were prepared by drop-casting the with acetonitrile diluted material on 200 *µ*m carbon-coated copper grids, followed by washing the grid several times with acetonitrile to remove the excess ionic liquid. The size distribution was determined manually or with the aid of the Gatan Digital Micrograph software from at least 50 individual particles.

Gas sensing properties of the sensor elements were characterized using a home-designed flow type sensing measurement system inside an aluminum chamber with precisely controlled temperature and atmosphere. The Ni@rGO doping of WO_3 samples was done by preparing a physical mixture of the WO_3 xerogel and Ni@rGO. At a pressure of 150 kPa, tablets were pressed from the powder, (diameter 10 mm, thickness 2.5 mm, weight 0.75 g), which were sintered in air at 450 °C (4 hours). Electrical resistance of samples WO_3, rGO/WO_3, 0.35 wt% Ni@rGO/WO_3 in the range of 20 °C – 240 °C was measured by the two-probe method in a

corundum cell using an Agilent 34401 digital multimeter. The cell was placed in a tube furnace with a temperature regulator. To enhance electrical conductivity and to improve contact Ag electrodes were deposited on parallel sides of the pellets. The measurement procedure was carried out as follows: The sensing element was placed into a preheated and thermostabilized chamber. Then the testing gas mixtures (10 ppm NO_2 and 35,000 ppm acetone in air) were injected into the chamber at a rate of 2 L/h during 10 min. And, finally, the chamber with the sensing element was refilled by air for another 10 min. After this, the measurement was repeated.

Magnetic measurements were carried out by the ponderomotive method with automatized installation for measuring magnetic characteristics and for determination of the magnetic impurities in substances by nondestructive testing method with precision to 0.01%. The measurement error for the magnetization relative to the mass of the measured samples is equal to ±0.005 Am^2/kg, for the magnetic susceptibility of known mass samples it is equal to $\pm 1 \cdot 10^{-11}$ m^3/kg.

Preparation of nanoparticles in ionic liquid

Nickel nanoparticles on rGO (Ni@rGO) were prepared in septum-sealed 10 mL CEM microwave-vessels in a CEM Discover microwave under argon atmosphere. $Ni(COD)_2$ (49.2 mg, 0.178 mmol) and rGO (10 mg) were suspended for 2 hours in the dried and deoxygenated IL (2 g [BMIm][NTf_2]) before microwave decomposition (230 °C, 10 min, 50 W) to obtain a dispersion of 0.5 wt-% of Ni-nanoparticles decorated on rGO in ionic liquid.

Supplementary data

Supplementary material related to this article can be found, in the online version, at doi: gives a comparison with other gas sensors.

Acknowledgements

Authors are thankful to the Deutsche Forschungsgemeinschaft (DFG) for financial support within the priority project SPP 1708 *"Material Synthesis Near Room Temperature"* through grant Ja466/31-1, Ja466/31-2. We thank the Ernst Ruska-Centre (Forschungszentrum Jülich GmbH, Jülich, Germany) and Dr. Juri Barthel for access to the TEM facility and technical support under project number ER-C D-066 and in the core-facilities program through grant MA 1280/40-1.

Declaration of Competing Interest

The authors declare that they have no known competing financial interests or personal relationships that could have appeared to influence the work reported in this paper.

[1] Mane, A. T.; Kulkarni, S. B.; Navale, S. T.; Ghanwat, A. A.; Shinde, N. M.; Kim, J.; Patil, V. B. *Ceram. Int.* **2014,** *40* (10), 16495–16502. doi:10.1016/j.ceramint.2014.08.001.

[2] Tian, W.; Liu, X.; Yu, W. *Applied Sciences* **2018,** *8* (7), 1118–1138. doi:10.3390/app8071118.

[3] Meng, F.-L.; Guo, Z.; Huang, X.-J. *Trends Anal. Chem.* **2015,** *68*, 37–47. doi:10.1016/j.trac.2015.02.008.

[4] Varghese, S. S.; Lonkar, S.; Singh, K. K.; Swaminathan, S.; Abdala, A. *Sens. Actuators, B* **2015,** *218*, 160–183. doi:10.1016/j.snb.2015.04.062.

[5] Basu, S.; Bhattacharyya, P. *Sens. Actuators, B* **2012,** *173*, 1–21. doi:10.1016/j.snb.2012.07.092.

[6] Nunes, D.; Pimentel, A.; Gonçalves, A.; Pereira, S.; Branquinho, R.; Barquinha, P.; Fortunato, E.; Martins, R. *Semicond. Sci. Technol.* **2019**, *34* (4), 43001–44001. doi:10.1088/1361-6641/ab011e.

[7] Wetchakun, K.; Samerjai, T.; Tamaekong, N.; Liewhiran, C.; Siriwong, C.; Kruefu, V.; Wisitsoraat, A.; Tuantranont, A.; Phanichphant, S. *Sens. Actuators, B* **2011**, *160* (1), 580–591. doi:10.1016/j.snb.2011.08.032.

[8] Sun, D.; Luo, Y.; Debliquy, M.; Zhang, C. *Beilstein J. Nanotechnol.* **2018**, *9*, 2832–2844. doi:10.3762/bjnano.9.264.

[9] Jeevitha, G.; Abhinayaa, R.; Mangalaraj, D.; Ponpandian, N.; Meena, P.; Mounasamy, V.; Madanagurusamy, S. *Nanoscale Adv.* **2019**, *1* (5), 1799–1811. doi:10.1039/C9NA00048H.

[10] Long, H.; Zeng, W.; Zhang, H. J. *Mater. Sci.: Mater. Electron.* **2015**, *26* (7), 4698–4707. doi:10.1007/s10854-015-2896-4.

[11] Xia, Y.; Li, R.; Chen, R.; Wang, J.; Xiang, L. *Sensors* **2018**, *18* (5), 1456–1477. doi:10.3390/s18051456.

[12] Mattinen, M.; Wree, J.-L.; Stegmann, N.; Ciftyurek, E.; Achhab, M. E.; King, P. J.; Mizohata, K.; Räisänen, J.; Schierbaum, K. D.; Devi, A.; Ritala, M.; Leskelä, M. *Chem. Mater.* **2018**, *30* (23), 8690–8701. doi:10.1021/acs.chemmater.8b04129.

[13] D'Anna, F.; Grilli, M. L.; Petrucci, R.; Feroci, M. *Metals* **2020**, *10* (4), 475. doi:10.3390/met10040475.

[14] Kukkola, J.; Mäklin, J.; Halonen, N.; Kyllönen, T.; Tóth, G.; Szabó, M.; Shchukarev, A.; Mikkola, J.-P.; Jantunen, H.; Kordás, K. *Sens. Actuators, B* **2011,** *153* (2), 293–300. doi:10.1016/j.snb.2010.10.043.

[15] Vasilopoulou, M.; Palilis, L. C.; Georgiadou, D. G.; Douvas, A. M.; Argitis, P.; Kennou, S.; Sygellou, L.; Papadimitropoulos, G.; Kostis, I.; Stathopoulos, N. A.; Davazoglou, D. *Adv. Funct. Mater.* **2011,** *21* (8), 1489–1497. doi:10.1002/adfm.201002171.

[16] Li, J.; Liu, X.; Cui, J.; Sun, J. *ACS applied materials & interfaces* **2015,** *7* (19), 10108–10114. doi:10.1021/am508121p.

[17] Gillet, M.; Aguir, K.; Lemire, C.; Gillet, E.; Schierbaum, K. *Thin Solid Films* **2004,** *467* (1-2), 239–246. doi:10.1016/j.tsf.2004.04.018.

[18] Gu, H.; Wang, Z.; Hu, Y. *Sensors* **2012,** *12* (5), 5517–5550. doi:10.3390/s120505517.

[19] Esfandiar, A.; Irajizad, A.; Akhavan, O.; Ghasemi, S.; Gholami, M. R. *Int. J. Hydrogen Energy* **2014,** *39* (15), 8169–8179. doi:10.1016/j.ijhydene.2014.03.117.

[20] Ramkumar, S.; Rajarajan, G. *Appl. Phys. A* **2017,** *123* (6). doi:10.1007/s00339-017-0983-5.

[21] van Tong, P.; Hoa, N. D.; van Duy, N.; Le, D. T. T.; van Hieu, N. *Sens. Actuators, B* **2016,** *223*, 453–460. doi:10.1016/j.snb.2015.09.108.

[22] Ji, H.; Zeng, W.; Li, Y. *Nanoscale* **2019,** *11* (47), 22664–22684. doi:10.1039/c9nr07699a.

[23] Eranna, G.; Joshi, B. C.; Runthala, D. P.; Gupta, R. P. *Crit. Rev. Solid State Mater. Sci.* **2004,** *29* (3-4), 111–188. doi:10.1080/10408430490888977.

[24] Woo, H.-S.; Kwak, C.-H.; Chung, J.-H.; Lee, J.-H. *Sens. Actuators, B* **2015,** *216*, 358–366. doi:10.1016/j.snb.2015.04.035.

[25] Xiao, X.; Zhou, X.; Ma, J.; Zhu, Y.; Cheng, X.; Luo, W.; Deng, Y. *ACS Appl. Mater. Interfaces* **2019,** *11* (29), 26268–26276. doi:10.1021/acsami.9b08128.

[26] Wang, T.; Huang, D.; Yang, Z.; Xu, S.; He, G.; Li, X.; Hu, N.; Yin, G.; He, D.; Zhang, L. *Nano-micro letters* **2016,** *8* (2), 95–119. doi:10.1007/s40820-015-0073-1.

[27] Mao, S.; Lu, G.; Yu, K.; Bo, Z.; Chen, J. *Adv. Mater.* **2010,** *22* (32), 3521–3526. doi:10.1002/adma.201000520.

[28] Li, Q.; Liu, W.; Cao, G.; Li, X.; Wang, X. *Appl. Phys. Lett.* **2016,** *108* (22), 221604–221607. doi:10.1063/1.4952619.

[29] Su, P.-G.; Peng, S.-L. *Talanta* **2015,** *132*, 398–405. doi:10.1016/j.talanta.2014.09.034.

[30] Yin, P. T.; Shah, S.; Chhowalla, M.; Lee, K.-B. *Chem. Rev.* **2015,** *115* (7), 2483–2531. doi:10.1021/cr500537t.

[31] Mirzaei, A.; Kim, S. S.; Kim, H. W. *J. Hazard. Mater.* **2018,** *357*, 314–331. doi:10.1016/j.jhazmat.2018.06.015.

[32] Zhang, J.; Zeng, D.; Wang, H.; Qin, Z.; Pang, A.; Xie, C. *Mater. Lett.* **2017,** *204*, 27–30. doi:10.1016/j.matlet.2017.06.008.

[33] Mahajan, S.; Jagtap, S. *Appl. Mater. Today* **2020,** *18*, 100483. doi:10.1016/j.apmt.2019.100483.

[34] Bhati, V. S.; Ranwa, S.; Rajamani, S.; Kumari, K.; Raliya, R.; Biswas, P.; Kumar, M. *ACS Appl. Mater. Interfaces* **2018,** *10* (13), 11116–11124. doi:10.1021/acsami.7b17877.

[35] Wang, T.; Hao, J.; Zheng, S.; Sun, Q.; Di Zhang; Wang, Y. *Nano Res.* **2018,** *11* (2), 791–803. doi:10.1007/s12274-017-1688-y.

[36] Le Hoa, T.; Tien, H. N.; van Luan, H.; Chung, J. S.; Hur, S. H. *Sens. Actuators, B* **2013,** *185*, 701–705. doi:10.1016/j.snb.2013.05.050.

[37] Jie, X.; Zeng, D.; Zhang, J.; Xu, K.; Wu, J.; Zhu, B.; Xie, C. *Sens. Actuators, B* **2015,** *220*, 201–209. doi:10.1016/j.snb.2015.05.047.

[38] Zhang, J.; Wu, J.; Wang, X.; Zeng, D.; Xie, C. *Sens. Actuators, B* **2017,** *243*, 1010–1019. doi:10.1016/j.snb.2016.12.062.

[39] Piloto, C.; Shafiei, M.; Khan, H.; Gupta, B.; Tesfamichael, T.; Motta, N. *Appl. Surf. Sci.* **2018,** *434*, 126–133. doi:10.1016/j.apsusc.2017.10.152.

[40] Singkammo, S.; Wisitsoraat, A.; Sriprachuabwong, C.; Tuantranont, A.; Phanichphant, S.; Liewhiran, C. *ACS Appl. Mater. Interfaces* **2015,** *7* (5), 3077–3092. doi:10.1021/acsami.5b00161.

[41] Ghosal, S.; Bhattacharyya, P. *CSIT* **2020. doi:**10.1007/s40012-020-00299-z.

[42] Esfandiar, A.; Ghasemi, S.; Irajizad, A.; Akhavan, O.; Gholami, M. R. *Int. J. Hydrogen Energy* **2012,** *37* (20), 15423–15432. doi:10.1016/j.ijhydene.2012.08.011.

[43] Chen, L.; Huang, L.; Lin, Y.; Sai, L.; Chang, Q.; Shi, W.; Chen, Q. *Sens. Actuators, B* **2018,** *255*, 1482–1490. doi:10.1016/j.snb.2017.08.158.

[44] Wang, Z.; Zhang, Y.; Liu, S.; Zhang, T. *Sens. Actuators, B* **2016,** *222*, 893–903. doi:10.1016/j.snb.2015.09.027.

[45] Davar, F.; Fereshteh, Z.; Salavati-Niasari, M. *J. Alloys Compd.* **2009,** *476* (1-2), 797–801. doi:10.1016/j.jallcom.2008.09.121.

[46] LaGrow, A. P.; Ingham, B.; Toney, M. F.; Tilley, R. D. *J. Phys. Chem. C* **2013,** *117* (32), 16709–16718. doi:10.1021/jp405314g.

[47] Wegner, S.; Rutz, C.; Schütte, K.; Barthel, J.; Bushmelev, A.; Schmidt, A.; Dilchert, K.; Fischer, R. A.; Janiak, C. *Chem. Eur. J.* **2017,** *23* (26), 6330–6340. doi:10.1002/chem.201605251.

[48] Chaban, V. V.; Fileti, E. E. *RSC Adv.* **2015,** *5* (99), 81229–81234. doi:10.1039/C5RA16857K.

[49] Marquardt, D.; Vollmer, C.; Thomann, R.; Steurer, P.; Mülhaupt, R.; Redel, E.; Janiak, C. *Carbon* **2011,** *49* (4), 1326–1332. doi:10.1016/j.carbon.2010.09.066.

[50] Schmitz, A.; Schütte, K.; Ilievski, V.; Barthel, J.; Burk, L.; Mülhaupt, R.; Yue, J.; Smarsly, B.; Janiak, C. *Beilstein J. Nanotechnol.* **2017,** *8*, 2474–2483. doi:10.3762/bjnano.8.247.

[51] Srivastava, S.; Jain, K.; Singh, V. N.; Singh, S.; Vijayan, N.; Dilawar, N.; Gupta, G.; Senguttuvan, T. D. *Nanotechnology* **2012,** *23* (20), 205501. doi:10.1088/0957-4484/23/20/205501.

[52] Qu, W.; Bao, H.; Zhang, L.; Chen, G. *Chem. Eur. J.* **2012,** *18* (49), 15746–15752. doi:10.1002/chem.201202913.

[53] Ashcroft, N. W.; Mermin, N. D. *Solid state physics*, Repr; Brooks/Cole Thomson Learning: South Melbourne, 2012.

[54] Bonhôte, P.; Dias, A.-P.; Papageorgiou, N.; Kalyanasundaram, K.; Grätzel, M. *Inorg. Chem.* **1996,** *35* (5), 1168–1178. doi:10.1021/ic951325x.

[55] Burrell, A. K.; Sesto, R. E. D.; Baker, S. N.; McCleskey, T. M.; Baker, G. A. *Green Chem.* **2007,** *9* (5), 449–454. doi:10.1039/b615950h.

[56] Hummers, W. S.; Offeman, R. E. *J. Am. Chem. Soc.* **1958,** *80* (6), 1339. doi:10.1021/ja01539a017.

[57] Luysberg, M.; Heggen, M.; Tillmann, K. *JLSRF* **2016,** *2* (A77). doi:10.17815/jlsrf-2-138.

[58] Thust, A.; Barthel, J.; Tillmann, K. *JLSRF* **2016,** *2* (A41). doi:10.17815/jlsrf-2-66.